Effect of lateral mobility of fluorescent probes in lipid mixing assays of cell fusion

Shi Kun Huang,* Ming Cheng‡ and Sek Wen Hui*
*Biophysics Dept., Roswell Park Memorial Institute Buffalo, New York 14263; and ‡Department of Physics and Astronomy, State University of New York at Buffalo, Buffalo, New York 14260 USA

ABSTRACT Monolayers of human erythrocytes, immobilized on a cover slip, were induced to fuse by polyethylene glycol (mol wt 8,000). The mobility of fluorescent probes, 1-oleoyl-2-[12-[(7-nitro-2,1,3-benzoxadiazol-4-*yl*)amino]dodecanoyl] phosphatidyl-choline (C_{12}-NBD-PC), from labeled cells to unlabeled cells was monitored by video-enhanced fluorescence microscopy. A dequenching curve was obtained from the measurement of fluorescence intensities of pairs of fused cells over time. The dequenching curve and the curve obtained from macroscopic measurements of a cell monolayer (described in the preceding article) were compared and discussed. The slow probe transfer rate between a pair of fused cells was explained by a diffusion model based on membrane area conservation and the geometry of the fusion lumen. An equivalent lumen between two fused cells, thought to be the main rate limitation of probe mobility after fusion, was calculated to be ~130 nm in diameter. Lumens of 75 nm in diameter were observed by electron microscopy. Thus, the rate of macroscopic fluorescence dequenching depends not only upon the fusion efficiency, but also upon the number of simultaneous fusion partners, the geometry of their contact points, and the lateral mobility of the fluorescent probes through these points. The relative fusion efficiency can be derived only from the saturation dequenching values.

INTRODUCTION

During the past decade a number of fluorescence assays have been designed to quantitate the fusion of phospholipid vesicles. Mixing of the membrane components, either labeled phospholipids or lipid-soluble probes, is one of these methods used for sensitive and continuous monitoring of the kinetics of the fusion process (Duzgunes et al., 1987; Hoekstra et al., 1984). The rate of fusion of vesicles in suspension is dependent upon the collision, aggregation, and fusion efficiencies (Nir et al., 1983). In most lipid-mixing experiments, the effect of diffusion of fluorescent probes in the membranes of the vesicles can be neglected, due to the small size of the vesicles (<1 μm).

In experiments using larger vesicles or cells, the diffusion of lipids in the membranes, rather than the fusion rate, can be the limiting step in kinetic assays. This is known as one of the slow artifacts (Silvius et al., 1988). By using a fluorescence photobleaching recovery technique, the diffusion coefficient of 3, 3'-dioctadecylindodicarbocyanine iodide in intact normal human erythrocytes was measured to be 8.2×10^{-9} cm^2/s at 25°C (Bloom and Webb, 1983). By measuring the movement of fluorescent lipid probes from a labeled human erythrocyte membrane to an unlabeled erythrocyte membrane, after electric-field-induced fuison, the average diffusion coefficient was found to be 3.8×10^{-9} cm^2/s at 25°C (Sowers, 1985). In this case, the perfect trap model was used to calculate the diffusion coefficient of fluorescent probes between two cells (Chao et al., 1981; Koppel, 1984). The use of the perfect trap model without the geometric factor is acceptable because the lumen is relatively large. However, in the case of adherent cells, the lumen can be very small, due to the conservation of membrane area, which is largely fixed on the substrate. The diffusion of the fluorescent probes from one cell to another is limited by the small size of the lumen between two fused cells. Only then the geometric factor becomes important (Weaver, 1983; Koppel, 1984).

In this paper, the fluorescence self-quenching relief and the prober mobility in pairs of 1-oleoyl-2-[12-[(7-nitro-2,1,3-benzoxadiazol-4-*yl*)amino]dodecanoyl] phosphatidyl-choline (C_{12}-NBD-PC) labeled and unlabeled cells, induced to fuse by poly (ethylene) glycol (PEG), was monitored by video-enhanced fluorescence microscopy. The lumen size between two fused cells was deduced and fluorescence dequenching curves were explained in terms of the geometric constraint.

MATERIALS AND METHODS

Fluorescence microscopy

Microscope glass coverslips were coated with alcian blue solution (0.7%) in 80°C for 15 min, then rinsed in distilled H_2O and dried. Human

Address correspondence to Dr. Sek Wen Hui.
Dr. Huang's present address is Cancer Research Institute, University of California at San Francisco, San Francisco, CA 94143

0006-3495/90/11/1119/08 $2.00

erythrocytes were labeled with C_{12}-NBD-PC as described in the preceding article. Washed erythrocytes, both labeled or unlabeled, were allowed to settle on the alcian blue-coated glass coverslip for 5 min. Cells were attached to the surface of the glass coverslip due to the positive charge of alcian blue. Unattached cells were removed by washing with Hanks Balanced Salt Solution (BSS) (Hanks and Wallace, 1949).

A Model BH2-RFL, Olympus fluorescence microscope was used to obtain both the phase contrast and fluorscence impages. A 100 X, S Plan Achromat Objective Lens was used for observation. For observing the C_{12}-NBD-PC fluorescence, an excitation filter combination (BP-490/ET-455) dichroic mirror DM-500, and emission filter 0-515 were applied. Neutral density filters were used to reduce the effect of photobleaching.

The flow-though chamber was made as depicted in Fig. 1. The glass coverslip with the attached cell monolayer was placed cellside down on the chamber. Silicone based vacuum grease was applied between the coverslip and the top of the chamber to prevent leaking after the chamber was filled with solution. The coverslip was secured by two spring holders to prevent movement and flotation during the changing of solutions. 35 wt% PEG was injected from tube A to fill the chamber. After 5 min, BSS was injected from tube A, and PEG was diluted and drained away from tube B, until most of the PEG was removed.

Image recording and analysis

Analogue images of samples were taken by a 66 series, silicon intensified camera (SIT camera) from Dage-MTI, Inc. (Michigan City, Ind.). Although the camera was provided with an automatic gain control, it was operated in the manual mode, to record the real intensity level during monitoring. To remain in the linear region of the transfer curve of the camera, the light source was maintained at an appropriate level by using neutral density filters.

The images from the SIT camera were recorded in extra-high-grade video cassette tapes in an AG-6050 time lapse video cassette recorder from Panasonic, Co. (Secaucus, NJ), to reduce intensity distortion during analogue signal recording.

Digital image processing and analysis was employed to enhance the appearance of the microscopic image, by increasing contrast and reducing noise, using a MaxVision AT-1 Image Processor (from Datacube, Inc., Peabody, MA). By increasing the gain of the analogue-to-digital converter, higher contrast images were obtained. 60 frames (at 30 frames per s) were averaged by a live low-pass filter to reduce the background noise.

To more clearly visualize changes in distribution and intensity of the fluorescence, all images were analyzed and displayed in pseudocolor. In essence, this consisted of the 256 gray tones (black = 1; white = 256) used by the image processor, being assigned color values from blue to green to purple to red, and having each color from dark to light divided into 11 steps. The image was visualized on a color monitor, and photographs were taken directly from the monitor screen.

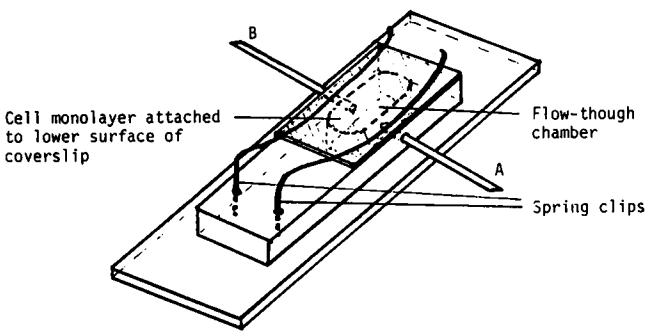

FIGURE 1 Schematic layout of the flowthrough chamber. The glass coverslip with the attached cell monolayer was placed cell side down on the chamber. A and B are fluid injecting and draining tubes.

To measure the change in fluorescence intensity of cells over time, a rectangle containing both a fluorescence labeled cell and an unlabeled cell was defined. The mean grey value of this region of interest (ROI) was obtained by image statistics. Because the background (cell-free) level is constant, the change in fluorescence of the cells under examination could be determined by calculating the change in the mean grey value of each ROI by comparing it to the respective ROI recorded at a previous or subsequent time point.

To compensate for the effect of photobleaching throughout the monitoring period, a parallel ROI within the same frame was defined. This consisted of a second rectangular region containing a single-fluorescence labeled cell and having the same cell surface to background ratio as the first ROI. The loss, in percent, of mean grey value within this control ROI from frame to frame was included as a bleaching-compensation factor in determining the final mean grey value of the respective experimental ROI.

Electron microscopy

Cell monolayer was treated with 35 wt% PEG in 4°C for 5 min, then was incubated with BSS at room temperature for 30 min. The cell monolayer was then fixed in 3% glutaraldehyde, and postfixed in 1% OsO_4. The cell monolayer on glass coverslip was dehydrated and embedded in epoxy resin with the glass coverslip at the bottom of an inverted capsule. After removing the glass coverslip, thin serial sections were cut from cell monolayers parallel to the surface facing the removed glass coverslip. The sections were stained and observed in a Siemens 101 microscope. More than 15 lumens were measured.

Model for probe diffusion through a small lumen

There are several theoretical studies to explain the diffusive movement of fluorescent probes from a labeled to an unlabeled cell after fusion. These theoretical treatments were based on the geometry of a fused pair of free-floating, spherical cells, which are assumed to take the shape of partially overlapping spheres. The degree of overlap is usually significant, resulting in a large ring of intersection or lumen (Koppel, 1984). In this geometry the probe movement is only slightly restricted by the geometry of the connecting ring, and the diffusion equation for constant cross section gives a good approximation (Koppel, 1984).

In our case of an adherent monolayer of spherical cells, there is no overlap between fused cells because the centers of the fused cells are fixed in space, and the diameters remain approximately the same before and after fusion.

Our model assumes a tunnel between two adjacent cells, the centers of which are $\sim 2R$ apart, R being the radius of a spherical cell. The tunnel has a circular cross section, and adjoins to cell surfaces at both ends with a continuous tangent. The tunnel surface is modeled to have two radii of curvature at the midpoint, namely, $(+u)$ = the smallest lumen radius, and $(-r)$ = the radius of the saddle circle. The geometry is depicted in Fig. 2.

The surface area of the tunnel and the two remaining portions of spherical cells, in polar coordinates, are, respectively,

$$2\int_0^{2\pi}\int_0^{\beta}(u + r - r\cos\theta)\, r d\theta\, d\phi$$

$$= 4\pi r(u + r)\beta - 4\pi r^2 \sin\beta, \quad (1)$$

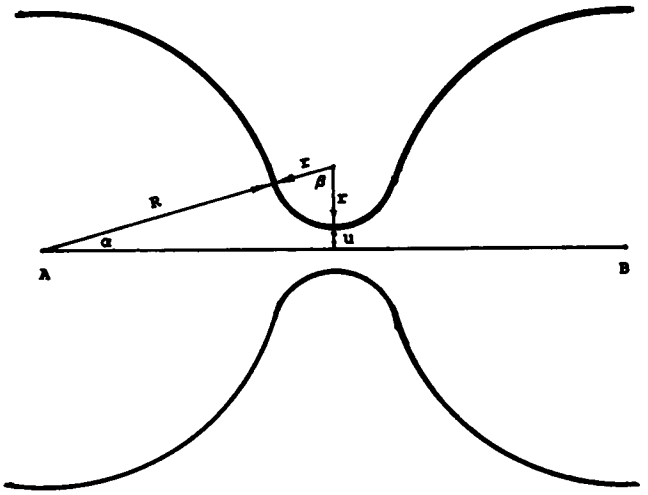

FIGURE 2 A surface conservation model shows two spherical cells each with radius R are conjoined with a lumen with minimum radius u and saddle point radius of curvature r. The spherical centers of the two cells are A and B, respectively. α is a characteristic angle which determines the lumen size.

and

$$2\int_0^{2\pi}\int_0^{\alpha}(R^2\sin\theta)\,d\theta\,d\phi = 4\pi R^2(1+\cos\alpha). \qquad (2)$$

By the conservation of surface area, the sum of these areas must equal the combined surface areas $8\pi R^2$ of the two spherical cells before fusion. Using the geometric relations

$$\beta = \pi/2 - \alpha,$$

and

$$R\sin\alpha = r + u - r\cos\beta, \qquad (3)$$

we solved the relationships between r, R, and u at the limit of small α. Taking $\sin\alpha \simeq \alpha$, $\cos\alpha \simeq 1 - \alpha^2/2$ and ignoring the second and higher powers of α in comparison to unity, we arrive at the following relations:

$$r \simeq (\pi/2)\alpha R \simeq \alpha R, \qquad (4)$$

and

$$u \simeq \alpha r. \qquad (5)$$

Thus, the luman radius may be calculated from the cell radius if α is known.

For diffusive motion of fluorescent probes along the narrow tunnel wall from the labeled-cell surface to the unlabeled one, the diffusion boundary length must be taken into account. The two-dimensional transport equation along the x direction through a variably bound surface with boundary length L is

$$\partial\sigma/\partial t = (1/L)[\partial(LJ)/\partial x], \qquad (6)$$

where

$$J = -D(\partial\sigma/\partial x)$$

is the surface flow, σ is the surface concentration of probes, and D is the 2-D diffusion coefficient. The diffusion equation through a variable cross length is then

$$\partial\sigma/\partial t = (1/L)\partial/\partial x(DL[\partial\sigma/\partial x])$$
$$= D(\partial^2\sigma/\partial x^2) - D/L(\partial L/\partial x)(\partial\sigma/\partial x). \qquad (7)$$

The second term at the righthand side defines the impedance to free diffusion motion by restrictions at small L. Even without the impedance term, Eq. 7 is already difficult to solve, for a simple geometry. An approximate solution in the form of

$$A_{(t)} = A_0\exp(-2Dt/R^2) = A_0\exp(-t/\tau) \qquad (8)$$

has been derived by Chao et al. (1981) for a "perfect trap" on a sphere. Here $A_{(t)}$ is the asymmetry index as defined by Poo (1981) as

$$A_{(t)} = [I_{(A,t)} - I_{(B,t)}]/[I_{(A,t)} + I_{(B,t)}], \qquad (9)$$

where fluorescence intensity $I_{(A,t)}$ and $I_{(B,t)}$ are correlated to the fluorescent probe concentration at points A and B (in Fig. 2) at time t, respectively. This relation can be applied to describe the unrestricted diffusion of fluorescent probes from one spherical cell to another through a large, infinitely thin lumen. τ for diffusion through large, thin lumen may be calculated from R and D (Koppel, 1984). Conversely, from measurements of τ and R, D can be deduced (Sowers, 1985).

For an imperfect trap of a given size, a mean transfer time,

$$\tau = R^2/D\gamma f, \qquad (10)$$

was deduced by Weaver (1983) where γf, is the product of the trapping probability and the geometric factor of the trap. The geometric factor is an important consideration in our model with the small tunnel acting as a trap (Weaver, 1983; Koppel, 1984). In this case

$$\gamma f \simeq 2\alpha^2.$$

The expression (10) then becomes

$$\tau \simeq R^2/2\alpha^2 D; \qquad (11)$$

τ may be deduced from Eq. 8 by expressing it at the logarithmic form

$$\ln A_{(t)} - \ln A_0 = -t/\tau$$
$$= -(2D\alpha^2/R^2)t. \qquad (12)$$

A plot of $\ln A_{(t)}$ against t would yield a slope $(-2D\alpha^2/R^2)$, from which $u = \alpha r = \alpha^2 R$ may be deduced if R and D are known.

RESULTS

A monolayer of cells at low density was placed on the flowthrough chamber and was continuously monitored by video-enhanced fluorescence microscopy. Each stage in the fusion process, involving single pairs of C_{12}-NBD-PC labeled and unlabeled cells, was recorded. The fluorescence micrographs of a typical fusion event, shown in Fig. 3, were enhanced by image processing. A small rectangular region of similar size and shape was defined in the same position (*center*) of each fluorescence image frame. Fig. 3, *A* and *B*, show the cells before PEG treatment. *A* is a fluorescence micrograph in which one C_{12}-NBD-PC labeled cell can be clearly seen in the lower left quadrant of the rectangular region. *B* is a phase-contrast micro-

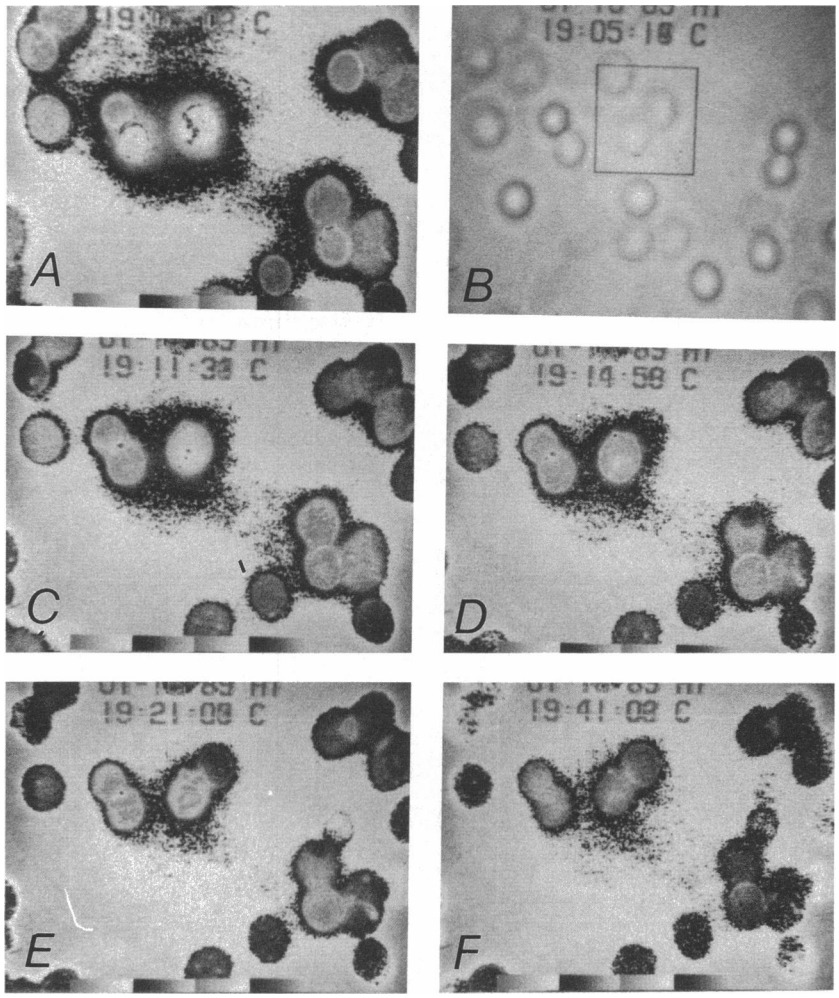

FIGURE 3 Different stages (*A–F*) in the fusion process of a single pair of C_{12}-NBD-PC labeled and unlabeled cells. (*A*) and (*B*), fluorescence and phase micrographs prior to PEG treatment. (*C–F*) fluorescence micrographs at time points (*C*) 30 s, (*D*) 230 s, (*E*) 10 min, and (*F*) 30 min after PEG removal. The fluorescence intensities were presented by pseudocolor. From lower to higher fluorescence intensities were assigned relative color values from blue to green, to purple to red, and having each color from dark to light divided into 11 steps. (The color photographs are rendered to black-and-white to reduced reproduction cost.) A small rectangular region of similar size and shape was defined in the same position (center) of each fluorescence image frame. Optical density histograms of the define region were used to plot the dequenching curve in Fig. 4.

graph in which the rectangular region is at the same position as that of *A*. The fluorescent cell is in the same position, and in the upper right quadrant is an unlabeled cell, which cannot be seen in *A*. Because of the thickness of the chamber, the phase contrast effect is poor. Gradual fluorescent probe transfer from the labeled to the unlabeled cell is shown in micrographs at (*C*) 0.5 min, and (*D*) 4 min after the dilution of PEG. Micrographs taken at (*E*) 10 min, and (*F*) 30 min after the dilution of PEG depict the diffusion of fluorescent probes proceeding to equilibrium in both cells.

During the fluorescent probe transfer from a labeled cell to an unlabeled cell throughout the fused pair, the total fluorescence intensity in the rectangular region increased due to the relief of fluorescence self-quenching. This enhancement of fluorescence intensity was due both to the dilution of the fluorescent probe as well as flip-flop (Huang and Hui, 1990).

Photobleaching was observed during monitoring of the cell fusion. An isolated, unfused cell, in the series of micrographs, changes gray levels (proportionally to fluorescence intensity) from light green and purple to dark green. This occurs even though the shutter was closed between the periodic recordings, and a neutral density filter was used to keep the light source moderate.

In our observation, no lipid transfer was detected between either isolated cells, or adjoining but unfused cells throughout the duration. For example, an unlabeled

cell in the upper left quadrant of the defined rectangular region can be seen in Fig. 3 *B* phase-contrast micrograph, but never shows up in fluorescent micrographs even at 30 min after PEG dilution. In the upper left corner of the phase-contrast micrograph of Fig. 3 *B*, the aggregation of two labeled cells with another unlabeled cell under treatment with PEG can be seen. At 30 min after dilution, no fluorescence probe transfer can be observed in the unlabeled cell, though it remained contacted and aggregated with labeled cells during the PEG treatment. In other words, if no fusion occurs, no fluorescence probe transfer is observed. It suggests that probe transferred across the medium, or through cell contiguity and aggregation without fusion, could not be detected in our experiment.

Probe dilution occurred not only among doublets, but also triplets and multiplets. On the right side of the screen in Fig. 3, the fluorescent probe was observed to move from labeled cells to an unlabeled cell, then passed on to another unlabeled cell through the many fusion points between the cells. This phenomenon must frequently occur when monolayers of high densities of cells (confluent) are subject to fusion treatment.

The curve *s* in Fig. 4 represents the average changes in fluorescence intensity measured from three series of micrographs containing pairs of fused cells, as shown in Fig. 3. Each point was obtained from the mean of the total grey level value, at a given time, after PEG dilution. Because of the photobleaching effect, each mean of the grey level value had been corrected by a control reference according to the method described in Materials and Methods.

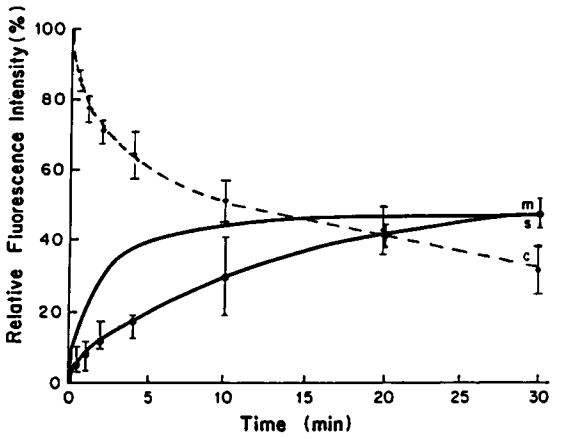

FIGURE 4 Curve *m*, is the sum of (*A*) and (*B*) in Fig. 10 of the previous paper, representing the dequenching of fluorescence from a monolayer of cells, due to fusion and the associated flip-flop. Curve *s* represents the average fluorescence intensities measured from three series of video micrographs of pairs of fusion cells, shown in Fig. 3. Both curves have been corrected for photobleaching effect, which is given in curve *c*.

Curve *m* in Fig. 4, represents the expected enhancement of the relative fluorescence intensity due to the relief of fluorescence self-quenching induced by fusion and associated flip-flop. It is the sum of curves *A* and *B* in Fig. 10 of the preceding article (Huang and Hui, 1990). In order to compare curve *m* with curve *s*, the latter was normalized by equating the final point to that of the former curve.

Fluorescent probe mobility following 35 wt% PEG induced cell fusion was quantitated in a flow-through chamber by video recording using a fluorescence microscope, and by image processing statistics. Fig. 5 is a sequence of micrographs of fluorescent probe diffusion from an originally C_{12}-NBD-PC labeled cell (second in lower left of Fig. 5 *A*) to an originally unlabeled cell (*below the labeled cell*), which cannot be seen at this stage, prior to PEG treatment. A line was defined from the upper to the lower cell across their spherical center. The vertical scale represents grey levels from 0–225, corresponding to the fluorescence intensity along this line. Fluorescent probe distribution was measured at (*B*) 2.5 min, (*C*) 5 min, (*D*) 7.5 min, (*E*) 10 min, (*F*) 15 min, (*G*) 20 min, (*H*) 25 min, and (*I*) 30 min after the dilution of 35 wt% PEG, and is depicted in Fig. 5. The profiles are of the corresponding fluorescence intensity along the defined line.

The asymmetry index was determined from five independent measurements by comparing the measured fluorescence intensity of the spherical centers of the two cells at a certain time. $A_{(t=0)}$ is defined by Eq. 9, using the normalized fluorescence intensities at points *A* and *B* (the spherical centers of two cells) before PEG treatment. The ln $A_{(t)}$ value is plotted against t in Fig. 6. The linear characteristic is apparent. The slope of the least square fitted curve is $0.00167 \pm 0.0004\ s^{-1}$. Using the diffusion coefficient D of $8.2 \times 10^{-9}\ cm^2/s$ at room temperature (Bloom and Webb, 1983) in Eq. 12, and our measured average radius of a human erythrocyte of 3.95 μm, the value for α^2 is determined to be 0.017 ± 0.004. By putting this value of α into Eqs. 4 and 5, the average diameter of the lumen is calculated to be 0.13 ± 0.03 μm.

In electron microscopic measurement, the average value of cross sections of lumens from serial sections of 15 fused cell pairs is 0.07 ± 0.03 μm. One of the sections is shown in Fig. 7.

DISCUSSION

Image processing and analysis provide a useful method to determine the relief of fluorescence self-quenching by dilution due to fusion between a single pair of fluorescence labeled and unlabeled cells. These microscopic measurements gave us an opportunity to distinguish the kinetics of

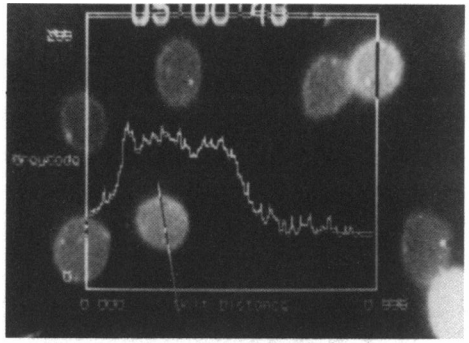

A) BEFORE THE DILUTION OF PEG.

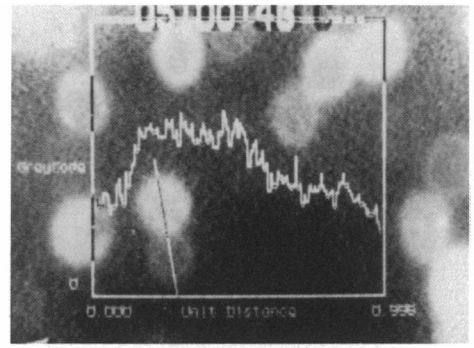

B) 0.25 MINUTES AFTER THE DILUTION OF PEG.

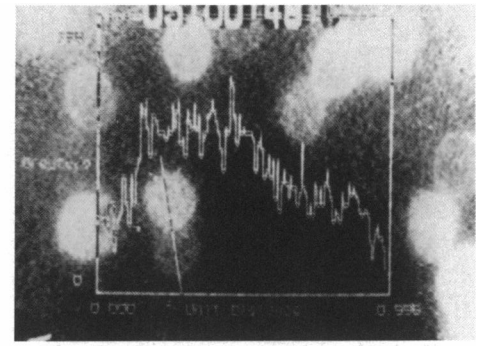

C) 5 MINUTES AFTER THE DILUTION OF PEG.

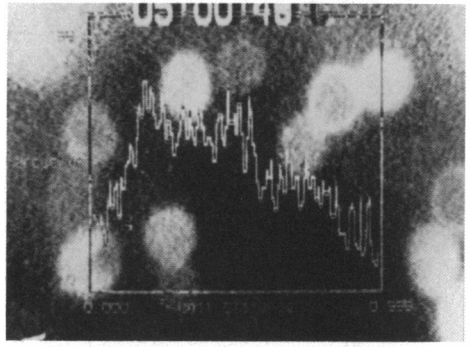

D) 7.5 MINUTES AFTER THE DILUTION OF PEG.

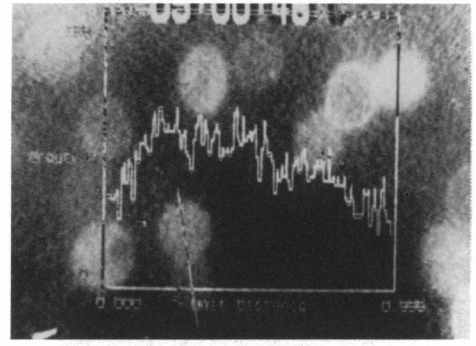

E) 10 MINUTES AFTER THE DILUTION OF PEG.

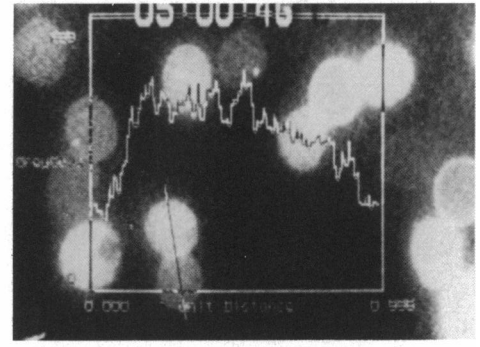

F) 15 MINUTES AFTER THE DILUTION OF PEG.

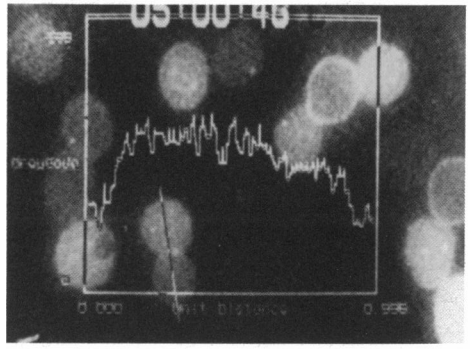

G) 20 MINUTES AFTER THE DILUTION OF PEG.

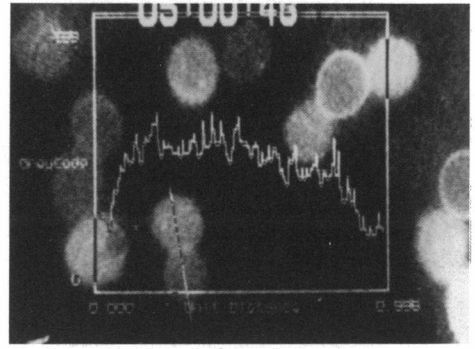

H) 25 MINUTES AFTER THE DILUTION OF PEG.

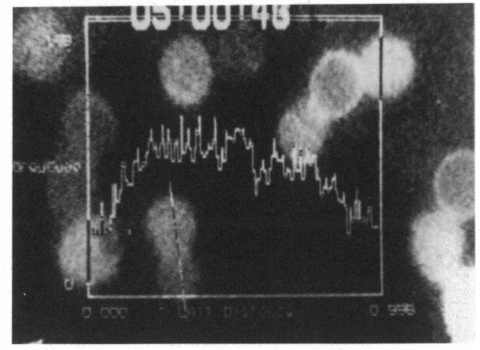

I) 30 MINUTES AFTER THE DILUTION OF PEG.

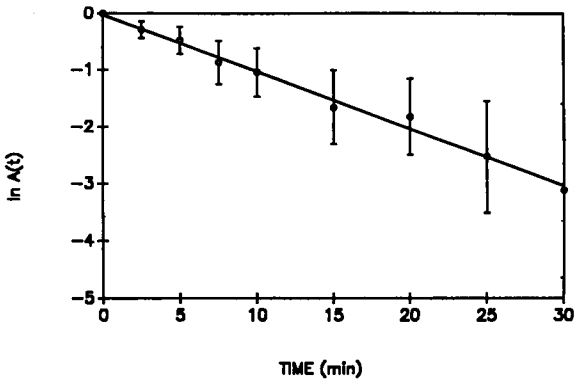

FIGURE 6 The plot of the natural logarithm of asymmetry indices as determined from the differences in the fluorescence intensities between the centers of each cell image (*A* and *B* in Fig. 2) after dilution of PEG. Each data point represents an average asymmetry index obtained from measurements on at least five cell pairs. The line represents linear regression by the least square method. The slope of 0.00167 s^{-1} gives the reciprocal of the characteristic diffusion time.

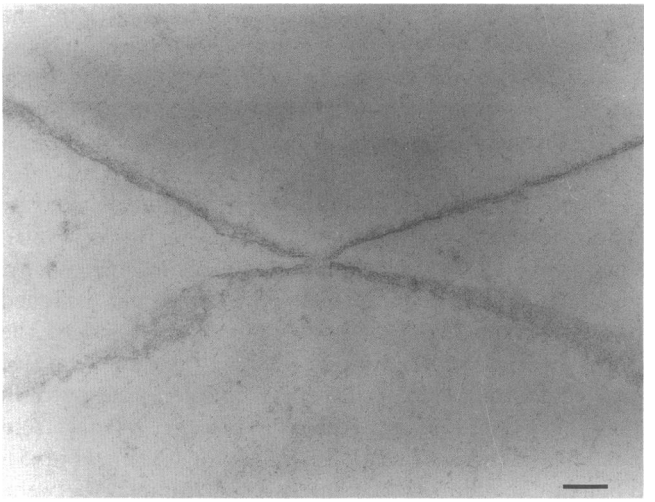

FIGURE 7 Electron micrograph of a typical section through one of the lumens between fused cells (*top and bottom*) in a monolayer. Bar, 1 μm.

microscopically determined fusion of individual cell pairs from the macroscopic measurement of whole monolayers of cells.

The macroscopically determined kinetics curve caused by fusion alone was compared with the curve obtained from microscopic measurements of a single pair of cells (Fig. 4). Clearly, the rates of the relative fluorescence intensity enhancement from these two techniques are different in the initial period following fusion. The observed kinetics are dominated by three major factors: (*a*) the efficiency of cell fusion, (*b*) the number of fusion partners, and (*c*) the rate of fluorescent probe mobility from a labeled cell to an unlabeled cell. In our observation, fusion occurred not only between two cells, but also among multiple cells. The confluent cell monolayer provided even more opportunities to form multiplets (shown in Fig. 3). The rate of fluorescence dequenching between one labeled cell and several unlabeled cells should be much faster than the rate between a single pair of a labeled and an unlabeled cell. Thus, the number and geometry of the cells in contact is an important consideration. The rate difference between the two kinetic curves in Fig. 4 is thought to be caused at least partially by the relief of fluorescence self-quenching from triple and other multiple fusion partners that were not measured microscopically in a single pair of fused cells. This factor strongly influenced the initial rate of fusion-mediated dequenching kinetics measured in confluent cell monolayers. In this case, the fusion rate, or the number of points of fusion, is dependent upon the fusion efficiency and the cell density. Eventually, the diffusion of the fluorescent probes between labeled and unlabeled cells will reach equilibrium. This is represented by the plateau region of the dequenching kinetics curve of a confluent cell monolayer. The saturation value corresponds to the magnitude of dequenching determined by the percentage of fusion.

The main rate-limiting step in the observed kinetics is due to the delay of fluorescence probes to diffuse through the point(s) or lumen(s) of contact between labeled and unlabeled cells. First, for swollen human erythrocytes, the average diameter is about 8 μm, much larger than the diameter of most lipid vesicles (<1 μm) which are commonly employed in experiments of artificial membrane fusion kinetics. Second, in our case, the lumen between two fused cells is very small, due to the restriction of movement of the cells attached to glass coverslips. The formation of the lumen is unlike that reported by Sowers (1985), in the electrofusion of freely suspended erythrocytes. In that case, a wide open lumen was observed between pairs of free-floating cells. In many other cases of

FIGURE 5 A sequence of micrographs of fluorescent probe diffusion from a C_{12}-NBD-PC labeled cell to an unlabeled cell after PEG-induced fusion was monitored by video-enhanced image processing. A line was defined from the upper to the lower cell across their spherical center. The horizontal scale of the rectangular frame corresponds to positions along this line. The vertical scale represents grey levels from 0 to 225, corresponding to the fluorescence intensity along this line. Fluorescence-intensity profiles were measured at (*B*) 2.5 min, (*C*) 5 min, (*D*) 7.5 min, (*E*) 10 min, (*F*) 15 min, (*G*) 20 min, (*H*) 25 min and (*I*) 30 min after the dilution of 35 wt% PEG.

cell fusion, only small lumens are formed, due to the restrictions of both surface tension and membrane cytoskeleton. From the observation of Ahkong and Lucy (1986), the cytoplasmic lumens between fused human erythrocytes in suspension, after dilution of 40 wt% PEG, were ~0.1 μm in width. The small lumen size was also reported in the fusion of human erythrocytes induced by nonhemolytic Sendai virus (Knutton and Bachi, 1980). Our measurements, by thin section electron microscopy, give similar lumen size between the fused cells attached on glass coverslips. This small lumen size is indeed the probe diffusion rate limitation between fused fluorescence labeled and unlabeled cells. This limitation was shown in the sequence of micrographs of fluorescence moving from a labeled membrane to an unlabeled membrane (Fig. 5). Though the fluorescence intensity asymmetry between two cells in each stage gradually changed, the fluorescence intensities within either the labeled or unlabeled individual cell is almost homogeneous. It suggests that the location of the restriction of the fluorescent probes diffusion is at the area where the two cells adjoin, i.e., lumen, rather than in the remaining areas of the cell membrane. Considering the approximations applied to the formulations to calculate the lumen size in our case, the results were surprisingly accurate, in comparison to electron microscopic measurement. The thin section measurement represents an average cross section diameter rather than $2u$, the maximum diameter at the central sectional plane. Therefore, some discrepancy is expected.

Our conclusions from analyzing the kinetics of cell fusion-mediated fluorescence dequenching are: first, the initial slope of the fluorescence dequenching curve is determined by both the number and the geometry of the contact points of fused cells, and the fusion efficiency. Second, the lumen size is the main rate limitation for the relief of fluorescence self-quenching after fusion. Third, only the final, saturated points of the kinetic curves represent the relative fusion efficiency. Therefore, caution should be used in the interpretation of fluorescence dequenching measurements of fusion-induced membrane mixing, especially in the case which the geometry of fusing partners is unknown.

We like to thank Mr. Edward Hurley for the serial thin section, and Dr. H. Slocum for the use of the SIT camera.

The work is supported by a grant GM 30969 from the National Institutes of Health.

REFERENCES

Ahkong, Q. F., and J. A. Lucy. 1986. Osmotic forces in artificially induced cell fusion. *Biochim. Biophys. Acta.* 858:206–216.

Bloom, J. A., and W. W. Webb. 1983. Lipid diffusibility in the intact erythrocyte membrane. *Biophys. J.* 42:295–305.

Chao, N. M., S. H. Young, and M. M. Poo. 1981. Localization of cell membrane components by surface diffusion into a "trap." *Biophys. J.* 36:139–153.

Duzgunes, N., T. M. Allen, J. Fedor, and D. Papahadjopoulos. 1987. Lipid mixing during membrane aggregation and fusion: why fusion assays disagree. *Biochemistry.* 26:8435–8442.

Hanks, J. H., and R. E. Wallace. 1949. Relation of oxygen and temperature in the preservation of tissues by refrigeration. *Proc. Soc. Exp. Biol. Med.* 71:196–200.

Hoekstra, D., T. de Boer, K. Klappe, and J. Wilschut. 1984. Fluorescence method for measuring the kinetics of fusion between biological membranes. *Biochemistry.* 23:5675–5681.

Huang, S. K., and S. W. Hui. 1990. The kinetics of fusion between human erythrocytes induced by polyethylene glycol. *Biophys. J.* 58:1109–1118.

Koppel, D. E. 1984. Lateral diffusion on fused cell doublets. *Biophys. J.* 46:837–838.

Knutton, S., and T. Bachi. 1980. The role of cell swelling and hemolysis in Sendai virus-induced cell fusion and the diffusion of incorporated viral antigens. *J. Cell Sci.* 42:153–167.

Nir, S., J. Bentz, J. Wilschut, and N. Düzgünes. 1983. Aggregation and fusion of phospholipid vesicles. *Prog. Surf. Sci.* 13:1–124.

Poo, M. M. 1981. In situ electrophoresis of membrane components. *Annu. Rev. Biophys. Bioeng.* 10:245–276.

Silvius, J. R., R. Leventis, and P. M. Brown. 1988. "Slow artifacts" in assays of lipid mining between membranes. *In* Molecular Mechanism of Membrane Fusion. S. Ohki, D. Doyle, T. Flanagan, S. W. Hui, and E. Mayhew, editors. Plenum Publishing Corp., New York.

Sowers, A. E. 1985. Movement of fluorescent lipid label from a labeled erythrocyte membrane to an unlabeled erythrocyte membrane following electric-field-induced fusion. *Biophys. J.* 47:519–525.

Weaver, D. L. 1983. Diffusion-mediated localization on membrane surfaces. *Biophys. J.* 4:81–86.